Data-Mined Continuous Hip-Knee Coordination Mapping With Motion Lag for Lower-Limb Prosthesis Control

Yang Lv, Jian Xu, Hongbin Fang, *Member, IEEE*, Xiaoxu Zhang, *Member, IEEE*, and Qining Wang, *Senior Member, IEEE*

***Abstract*— Trajectory planning of the knee joint plays an essential role in controlling the lower limb prosthesis. Nowadays, the idea of mapping the trajectory of the healthy limb to the motion trajectory of the prosthetic joint has begun to emerge. However, establishing a simple and intuitive coordination mapping is still challenging. This paper employs the method of experimental data mining to explore such a coordination mapping. The coordination indexes, i.e., the mean absolute relative phase (MARP) and the deviation phase (DP), are obtained from experimental data. Statistical results covering different subjects indicate that the hip motion possesses a stable phase difference with the knee, inspiring us to construct a hip-knee Motion-Lagged Coordination Mapping (MLCM). The MLCM first introduces a time lag to the hip motion to avoid conventional integral or differential calculations. The model in polynomials, which is proved more efficient than Gaussian process regression and neural network learning, is then constructed to represent the mapping from the lagged hip motion to the knee motion. In addition, a strong linear correlation between hip-knee MARP and hip-knee motion lag is discovered for the first time. By using the MLCM, one can generate the knee trajectory for the prosthesis control only via the hip motion of the healthy limb, indicating less sensing and better robustness. Numerical simulations show that the prosthesis can achieve normal gaits at different walking speeds.**

***Index Terms*— Trajectory planning, prosthesis control, lower limb coordination, MARP, motion lag.**

Manuscript received November 30, 2021; revised April 21, 2022; accepted May 31, 2022. Date of publication June 3, 2022; date of current version June 14, 2022. This work was supported in part by the National Key Research and Development Project of China under Grant 2018YFB1307305, in part by the National Natural Science Foundation of China under Grant 11902077, and in part by the Shanghai Sailing Program under Grant 19YF1403000. *(Corresponding author: Xiaoxu Zhang.)*

This work involved human subjects or animals in its research. Approval of all ethical and experimental procedures and protocols was granted by the Ethics Committee at the Fudan University, China, under Application No. FE21124 on 16 August 2021.

Yang Lv is with the Academy for Engineering and Technology, Fudan University, Shanghai 200433, China (e-mail: lvy21@m.fudan.edu.cn).

Jian Xu and Hongbin Fang are with the Shanghai Engineering Research Center of AI and Robotics, and the Academy for Engineering and Technology, Fudan University, Shanghai 200433, China (e-mail: jian_xu@fudan.edu.cn; fanghongbin@fudan.edu.cn).

Xiaoxu Zhang is with the Engineering Research Center of AI and Robotics, the MOE Frontiers Center for Brain Science, and the Academy for Engineering and Technology, Fudan University, Shanghai 200433, China (e-mail: zhangxiaoxu@fudan.edu.cn).

Qining Wang is with the College of Engineering, Peking University, Beijing 100871, China (e-mail: qiningwang@pku.edu.cn).

This article has supplementary downloadable material available at https://doi.org/10.1109/TNSRE.2022.3179978, provided by the authors.

Digital Object Identifier 10.1109/TNSRE.2022.3179978

I. Introduction

FOR the transfemoral amputees, wearing a lower-limb prosthesis is crucial to regain their walking capability. The powered knee prosthesis aims to move in a way that a healthy knee moves. There are mainly two methods for controlling a powered knee prosthesis for this aim. One is the impedance control based on a finite state machine (FSM) [1], [2]. The FSM-based impedance control divides the entire gait cycle into several gait phases (usually 4 or 5) and sets different impedance parameters in each gait phase. This control method is mainly used in commercial and prototypic prostheses. However, the number of control parameters is usually 10∼20, making parameter adjustments cost a considerable workload [3]. To address this challenge, Wen *et al.* [4], [5] design reinforcement learning (RL) supplementary control, which can synchronously tune 12 impedance control parameters and generate variant control parameter settings. In another way, Shorter and Rouse [6] estimate the ankle impedance in each gait phase by experiments and use the estimated impedance to control an ankle prosthesis. The other method for prosthesis control is the position control based on a reference trajectory. The position control framework generates a reference trajectory and then uses a low-level controller to minimize the error between the actual trajectory and the reference trajectory. This method does not need to divide the gait cycle into several phases, significantly reducing the number of control parameters. For the position control framework, the key problem lies in the trajectory planning of the knee joint.

The reference trajectory for position control is obtained through the gait experiments of healthy subjects in advance [7]. However, the experiments cannot cover all gait parameters (walking speed, step length, etc.) and body parameters (height, weight, etc.). This fact implies that the reference trajectory suitable for individualized gait and body parameters should be planned. Focusing on this issue, researchers employ many curve fitting methods (such as spline fitting [8], Gaussian process regression (GPR) [9], Fourier series fitting [10], etc.) to generate the reference trajectory. They further use the generated trajectory for gait treatment of severely affected patients (such as hemiplegic patients and stroke patients) and achieve effective results [11]. However, when the case comes

to the position control of the lower-limb prosthesis, forcing the prosthesis to move according to the reference trajectory seems unreasonable because it ignores the role of the amputees' healthy limbs in co-realizing the gait. Other research further reveals that the lower limbs show good coordination in a comfortable and efficient walking mode [12]. Thus, the coordination between the healthy limb and the prosthesis should be considered in trajectory planning.

In modeling the coordination relationship between the healthy and prosthetic limbs, the trajectory of the healthy limb is often treated as input, and the reference trajectory of the prosthesis is the output. One commonly used method to establish this mapping is the data-driven method (such as Random Forest Model [13] and Recurrent Neural Network [14]) due to its good performance in finding the non-empirical relationship between several related physical quantities. However, the mappings established by the conventional data-driven method may have two drawbacks. First, the mappings include trajectories of nearly all healthy limb joints as inputs, which means quite a lot of sensors need to be attached to the healthy limb. Second, the mappings need to train a large number of parameters. The calculation burden will be a big problem for the online deployment of prosthesis control. Thus, for the real-time trajectory planning of the prosthesis, a simple and intuitive mapping with a minimum number of sensors is required.

To achieve this goal, Valley *et al.* [15] propose a *complementary limb motion estimation* method (CLME) based on statistical regression to establish the mapping from the hip and knee motion of the healthy limb to the knee motion of the prosthesis. Later, an amputee subject successfully walks at different speeds and climbs stairs with the CLME-controlled knee prosthesis [16]. It is worth noting that only the healthy limb's hip and knee sensor signals are used in the CLME method. Some research further decreases the number of sensor inputs. Eslamy *et al.* [17] only use the hip angle and angular velocity to obtain the knee angle by Gaussian Process Regression (GPR), making the RMSE lower than 5°. Quintero *et al.* [18] use the hip angle and angular velocity (or angular integral) to build a phase variable for characterizing the reference knee angle, allowing three transfemoral amputees to walk naturally at different speeds and slope conditions. However, time-differentiating the joint angle to obtain angular velocity often amplifies the noise sensitivity of mapping. In fact, constructing coordination mapping may not require the velocity term or the integral term. For example, the coordination relationship between the left and right knee motion can be described only by introducing a phase difference of 180°. It enlightens us to construct a mapping without the velocity term by introducing a coordination phase difference parameter.

The phase difference is always a vital index in joint coordination research. The most commonly used index to describe the lower limb coordination is the *continuous relative phase* (CRP). CRP is derived from the difference between two joints' phase angles [19]. Furthermore, the *mean absolute relative phase* (MARP) and *deviation phase* (DP) can be derived based on CRP to evaluate joint coordination better. MARP [20] is defined by calculating the mean value of CRP over the entire gait cycle, and DP [21] is determined by calculating the mean value of the CRP's standard deviation to measure the stability of joint coordination. The smaller DP is, the more stable the joint coordination exists. Based on these two indexes, researchers compare the lower limb coordination of subjects of different ages [19], body shapes [22], walking speeds [23], and walking situations [20] (level-ground walking, up and downstairs, up and down slopes, etc.). However, few studies use these indexes to establish coordination mapping.

In general, a simple and intuitive coordination mapping is necessary for the online deployment of prosthesis control. Lack of comprehension of lower-limb coordination affects the establishment of a simple and intuitive coordination mapping. Meanwhile, the existing coordination research on the quantitative description of MARP and DP indexes is not used to establish a coordination mapping. Thus, there is a knowledge gap between the study of lower-limb coordination and the establishment of coordination mapping. This paper aims to fill this knowledge gap and apply coordination mapping to the position control of the knee prosthesis.

The established coordination mapping has three highlights. a) It only needs hip motion sensing and does not require integral or differential calculations. This feature saves the burden of information collection and processing in prosthesis control. b) The parameter introduced in this mapping, namely *motion lag*, can be directly estimated from the gait period and the walking speed. This feature simplifies the lower-limb prosthesis control. c) The established mapping can adapt to different individuals and walking speeds to some extent. This feature implies broad adaptability to various working conditions.

The structure of this paper is arranged as follows. In Section II, the gait experiments are conducted to get the coordination indexes. Then, the law of the lower limb coordination is analyzed. In Section III the hip-knee MLCM is established and analyzed. In Section IV, a specific method of applying the hip-knee MLCM to the real-time trajectory generation of the knee prosthesis is given and verified on the simulation platform. Finally, in Section V, we discuss the results of our method.

II. Preliminaries and Motivation

This section mainly clarifies the motivation for hip-knee coordination mapping based on the following hypothesis:

Hypothesis: There is a stable coordination phase difference between hip and knee over the entire gait cycle when walking at uniform speeds.

A. Experimental Protocol

Five males and five females (mean±std. age: 24.3±1.8 years, height: 1.71±0.07 m, weight: 58.15±6.33kg, BMI: 20.28±1.87) were invited to participate in this experiment. They all have good sports abilities and do not have any musculoskeletal injuries. This study was approved by the Ethics Committee at the Fudan University, China (No.

TABLE I
SUBJECT CHARACTERISTICS OF THE EXPERIMENT

Subject	Gender	Age	Weight (kg)	Height (m)	BMI
1	Female	24	49.75	1.66	18.05
2	Female	23	51.25	1.60	20.02
3	Female	24	49.55	1.62	18.88
4	Female	25	56.45	1.72	19.08
5	Female	22	56.20	1.68	19.91
6	Male	25	68.05	1.74	22.48
7	Male	23	66.10	1.76	21.34
8	Male	24	59.75	1.74	19.74
9	Male	24	63.85	1.71	21.84
10	Male	29	60.55	1.85	17.69

FE21124) on 16 Aug 2021. The aims and details of the protocol were fully explained to the subjects with the signing of written informed consent. Subject characteristics are given in Table I.

Each participant performed five walking tests on a treadmill at five walking speeds (2.5, 3.5, 4.5, 5.5, 6.5 km/h, denoted as WS1, WS2, WS3, WS4, WS5). The data was recorded for two minutes after the participant reported adapting to the current walking speed for each test. Then, the participant rested for another two minutes between tests. Nineteen markers were stuck on the subject based on the rule of the Helen-Hayes Model [24]. Markers' movement was recorded at a sampling rate of 120 Hz via the OptiTrack motion capture system. According to Helen Hayes Model, the hip, knee, and ankle joint trajectories in the sagittal plane were extracted.

B. Data Processing

For a time-discrete curve $\theta(t_i)$, where $t_i \in [0, T]$ and T is the gait period, its phase angle can be extracted by the Hilbert transform [25], i.e.

$$\varphi(t_i) = \arctan\left(\mathscr{H}[\theta_c(t_i)]/\theta_c(t_i)\right), \tag{1}$$

where $\mathscr{H}[\cdot]$ means the Hilbert transform of a signal. $\theta_c(t_i)$ is the zero-centered signal defined as

$$\theta_c(t_i) = \theta(t_i) - (\max(\theta) + \min(\theta))/2, \tag{2}$$

where $\max(\theta)$ and $\min(\theta)$ indicate the maximum and the minimum of $\theta(t_i)$ over one gait cycle.

Based on Eq. (1), this study defines the CRP between two joint motions as the phase angle of the proximal joint subtracting that of the distal joint. According to the distance from the joints to the main body, the hip joint is the most proximal, followed by the knee joint, and the ankle joint is the most distal. For example, the hip-knee CRP, denoted by $\phi_{\text{hip-knee}}$, is calculated by subtracting the knee phase angle from the hip phase angle.

$$\phi_{\text{hip-knee}}(t_i) = \varphi_{\text{hip}}(t_i) - \varphi_{\text{knee}}(t_i). \tag{3}$$

Eq. (3) indicates the continuous relative phase between the hip and knee angles. Especially, a 0° or 360° CRP means completely in-phase motion between the hip and knee joints, and a 180° CRP represents completely out-of-phase. By referring to Eq. (3), $\phi_{\text{knee-ankle}}$ and $\phi_{\text{hip-ankle}}$ can be calculated and explained in the same way. Furthermore, averaging the CRP in n gait cycles yields the averaged CRP Φ:

$$\Phi(t_i) = \frac{1}{n}\sum_{j=1}^{n}\phi\left(t_{i,j}\right), \tag{4}$$

where j indicates the j^{th} gait cycle and $t_{i,j} = t_i + (j-1)T$. By calculating the standard deviation of the CRP at each time point, the CRP variability Θ can be obtained:

$$\Theta(t_i) = \sqrt{\frac{1}{n-1}\sum_{j=1}^{n}\left(\phi\left(t_{i,j}\right) - \Phi(t_i)\right)^2}. \tag{5}$$

Averaging Φ and Θ over the gait cycle further yields MARP and DP:

$$\begin{aligned} \text{MARP} &= \bar{\Phi}(t_i), \\ \text{DP} &= \bar{\Theta}(t_i), \end{aligned} \tag{6}$$

MARP indicates the phase difference between two joints and has a similar physical meaning to CRP. When MARP equals 0° or 360°, the joints' motions are in phase on average over the entire gait cycle. When MARP equals 180°, the joints' motions are out-of-phase on average over the entire gait cycle. DP indicates the variability of joint coordination. A smaller DP means more stable coordination between the joints.

This study employs MATLAB (version 2020b, MathWorks, Natick, MA, USA) to process the detailed calculations defined by Eqs. (1)-(6). MARP and DP values of hip-knee, knee-ankle, and hip-ankle are calculated for the lower limb motion of all ten subjects at five walking speeds. To figure out the effects of the gait phase on MARP and DP, we also calculate MARP and DP values over the stance phase, swing phase, and entire gait cycle, respectively. So, there are 450 MARP values and 450 DP values (10 subjects *5 speeds *3 gait phases *3 coordinations). The calculated data is grouped in speed for joint coordination evaluation. The angle of the thigh relative to the gravitational direction (anticlockwise +) is used to describe the hip motion, and the angle between the thigh and the shank (flexion +) is adopted to represent the knee motion. Besides, the angle of dorsiflexion or plantar flexion (dorsiflexion +) indicates the ankle motion.

The MARP and DP results calculated by MATLAB are then given into SPSS (version 20, IBM Corp, Armonk, NY, USA) for further statistical analysis. Firstly, the outliers of the calculated MARP (15 out of 450) and DP (42 out of 450) values are removed because outliers may mislead the statistical results. Secondly, the normality of the data is tested. If the data obey the normal distribution, the homogeneity test of variance will be further carried out. If the data variance is homogeneous, analysis of variance (ANOVA) will be used to detect the effects of speed on MARP and DP. Otherwise, the Games-Howell test will be used. If the data does not obey the normal distribution, a non-parametric test (Kruskal-Wallis H test) will be carried out to detect the effects of speed and gait phase on MARP and DP. The significance level of the results is set at $p < 0.05$.

C. Statistical Results

Table II indicates that the p-values of MARP with respect to different walking speeds are all smaller than 0.05. This

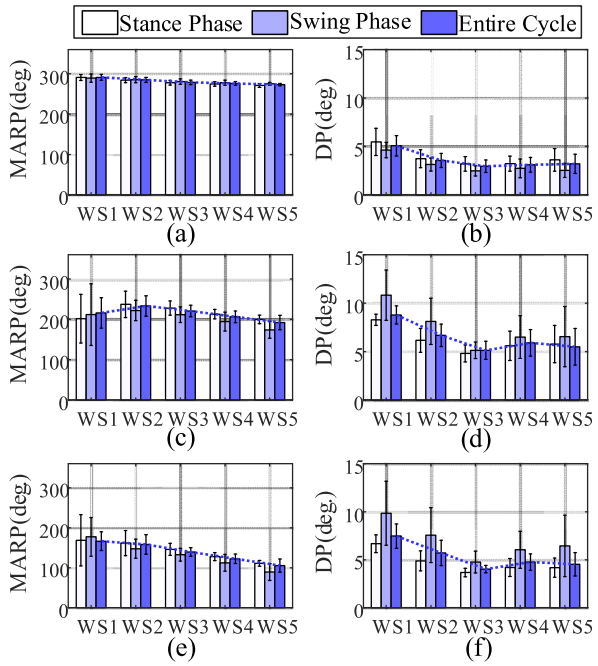

Fig. 1. Hip-knee, knee-ankle, hip-ankle MARPs and DPs, where the error bar indicates standard deviation between subjects. (a) Hip-knee MARP; (b) Hip-knee DP; (c) Knee-ankle MARP; (d) Knee-ankle DP; (e) Hip-ankle MARP; (f) Hip-ankle DP.

TABLE II
EFFECTS OF WALKING SPEED ON MARP AND DP (EVALUATED BY P-VALUE)

		Total Period	Stance Phase	Swing Phase
MARP	Hip-knee	<0.0001	<0.0001	0.001
	Knee-ankle	<0.0001	<0.0001	<0.0001
	Hip-ankle	<0.0001	<0.0001	<0.0001
DP	Hip-knee	<0.0001	0.002	<0.0001
	Knee-ankle	<0.0001	<0.0001	0.001
	Hip-ankle	<0.0001	<0.0001	0.014

feature illustrates that walking speed has a significant effect on interlimb MARP. In Fig.1a, c, and e, one can find that except for knee-ankle MARP at WS1, the MARP values of arbitrary two joints decrease with the walking speed increase. Besides, hip-knee, knee-ankle, and hip-ankle MARP values decrease at different ranges. Fig. 1a shows that the range of hip-knee MARP is 18.01°, which is significantly smaller than that of knee-ankle (41.01°, Fig.1c) and hip-ankle MARP (60.94°, Fig.1e).

Table II also indicates that walking speed significantly affects interlimb DP values. For example, in Fig.1b, d, and f, one can find that the DP values of arbitrary two joints at WS3 are significantly smaller than those at other walking speeds, which implies the coordination stability is the best at WS3. In fact, WS3 (4.5 km/h) is the closest to the normal walking speed of human adults (1.26 m/s≈4.5 km/h according to [23]). In other words, one can achieve the best coordination stability at normal walking speed. In addition, the hip-knee DP (2.96° ∼ 5.07 °) is generally smaller than the knee-ankle DP (5.13° ∼ 8.79 °) and hip-ankle DP (4.02° ∼ 7.47 °). Thus, the hip-knee phase difference is the most stable in lower-limb coordination.

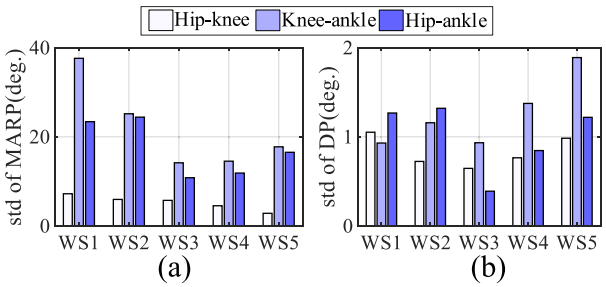

Fig. 2. Standard deviations of (a) MARP and (b) DP through entire gait cycle between different subjects.

Table III indicates that the gait phase does not significantly affect interlimb MARP and DP values, suggesting that the coordination phase difference is consistent in the stance and swing phases. Thus, the coordination mapping can be realized time-continuously over the entire gait cycle.

D. Motivation for Hip-Knee Coordination Mapping

Fig.2 shows the standard deviations of MARP and DP between different subjects. As can be seen, the standard deviation of hip-knee MARP is much smaller than that of the knee-ankle and hip-ankle MARPs. This feature means the hip-knee coordination phase difference has strong consistency and regularity between different subjects. Unlike the MARP results, the standard deviation of hip-knee DP is not always the smallest, e.g., WS1 and WS3, but maintains at a low level ($0.83 \pm 0.17°$). Thus, hip-knee coordination variability is also consistent among different subjects. The above analysis reveals that the hip-knee coordination relationship, especially the coordination phase difference represented by MARP, is not easily affected by individual differences. Combined with the analysis in the previous subsection, the hypothesis is validated. Hence, a hip-knee coordination mapping may be established by considering the coordination phase difference.

III. HIP-KNEE MOTION-LAGGED COORDINATION MAPPING

According to the analysis in subsection II.D, there is a stable phase difference between the hip and knee joint motions. This phase difference causes the hip joint and the knee joint to move with a constant time interval, called the hip-knee motion lag, from the perspective of time history. If the hip motion can be shifted backward with the hip-knee motion lag, it will be easier to establish the coordination mapping because the shifted hip motion and the knee motion are completely in-phase or out-of-phase. This section is carried out by developing such a mapping and analyzing it.

A. MLCM: Motion-Lagged Coordination Mapping

We introduce three candidates for the form of MLCM. The first is an n-order ($n = 2,3,4,5$) polynomial.

$$\tilde{y}(t) = \sum_{i=0}^{n} C_i x^i (t - \tau), \tag{7}$$

TABLE III
EFFECTS OF GAIT PHASE ON MARP AND DP, THE P-VALUES ARE OBTAINED BY COMPARING THE MARP AND DP RESULTS OVER STANCE PHASE AND SWING PHASE WITH THOSE OVER ENTIRE GAIT CYCLE

		WS1 p-value		WS2 p-value		WS3 p-value		WS4 p-value		WS5 p-value	
		Stance	Swing	Stance	Swing	Stance	Swing	Stance	Swing	Stance	Swing
MARP	Hip-knee	0.921	0.640	0.854	0.877	0.775	0.480	0.429	0.473	0.251	0.224
	Knee-ankle	0.612	0.870	0.508	0.369	0.344	0.275	0.331	0.616	0.450	0.940
	Hip-ankle	0.441	0.414	0.820	0.359	0.312	0.300	0.296	0.231	0.370	0.084
DP	Hip-knee	1.000	0.334	0.635	0.219	0.474	0.096	0.759	0.379	0.257	0.096
	Knee-ankle	0.277	0.070	0.420	0.164	0.514	0.895	0.660	0.498	0.769	0.462
	Hip-ankle	0.198	0.099	0.193	0.134	0.661	0.126	0.191	0.086	0.517	0.129

where $\tilde{y}(t)$ is the normalized mapped knee motion, $x(t-\tau)$ the normalized shifted hip motion, τ the hip-knee motion lag, and C_i the polynomial coefficient to the i^{th} order.

The second candidate is an RBF neural network[26], which uses the Gaussian function[27] as its activation function. The number of neurons is set to be 5. The third candidate is a GPR model, which is identical to that in [17] except for a different input (inputs in [17]: hip angle and angular velocity, our input: normalized shifted hip angle). These two candidates are chosen as the state of the art because they are widely used to fit curves and achieve good results in recent years.

The three candidates mentioned above will use the same experimental data to construct our MLCM. Their performances will be evaluated based on prediction accuracy and time, and the best-performing candidate will be used as the final form of MLCM.

The entire process of constructing the MLCM is shown in Fig.3(a). First, the normalized hip motion is shifted backward with a given lag τ. Then, parameter regression is conducted to map the normalized shifted backward hip motion to the normalized experimental knee motion. The regression strategies for polynomial, RBF, and GPR are the least square method, gradient descent method, and Bayesian Optimization, respectively. Finally, the k-means clustering algorithm is employed to find the center points and standard variances of the RBF network.

After parameter regression, the normalized mapped knee motion is obtained. Then, we come to the most important step of finding the best-fitted motion lag. The following reward function, denoted as r, is defined to evaluate the motion lag fitness.

$$r(\tilde{y}, y) = \left|\mathrm{Cov}(\tilde{y}, y) \Big/ \left(\sqrt{\mathrm{D}(\tilde{y})}\sqrt{\mathrm{D}(y)}\right)\right| \in [0, 1], \quad (8)$$

where

$$\mathrm{Cov}(\tilde{y}, y) = \frac{1}{\mathrm{T}}\int_0^{\mathrm{T}} \tilde{y}y dt - \left(\frac{1}{\mathrm{T}}\int_0^{\mathrm{T}} \tilde{y} dt\right)\left(\frac{1}{\mathrm{T}}\int_0^{\mathrm{T}} y dt\right),$$

$$\mathrm{D}(\tilde{y}) = \frac{1}{\mathrm{T}}\int_0^{\mathrm{T}} \tilde{y}^2 dt - \left(\frac{1}{\mathrm{T}}\int_0^{\mathrm{T}} \tilde{y} dt\right)^2,$$

$$\mathrm{D}(y) = \frac{1}{\mathrm{T}}\int_0^{\mathrm{T}} y^2 dt - \left(\frac{1}{\mathrm{T}}\int_0^{\mathrm{T}} y dt\right)^2,$$

here y is the measured signal of knee motion, and T represents the gait period time. The larger the value of $r(\tilde{y}, y)$, the stronger the consistency between the two signals, and the better the motion lag fitness is. To determine the optimal motion lag, τ is traversed from 0 to T, and then the largest $r(\tilde{y}, y)$ is selected. The corresponding τ is determined to be the motion lag used in the mapping, and the corresponding regression results determine the mapping parameters.

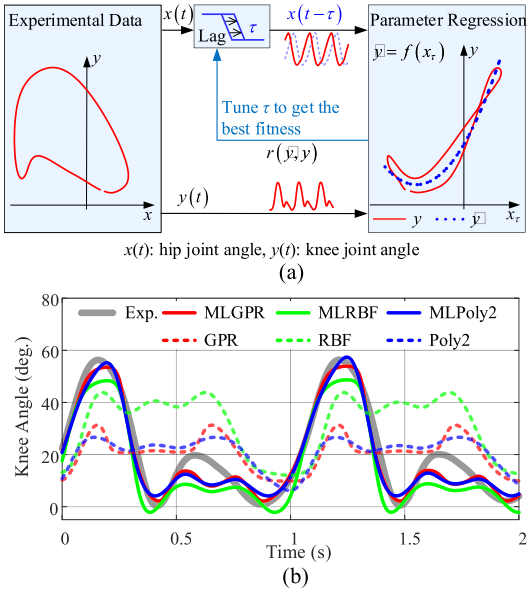

Fig. 3. (a) Flowchart of hip-knee MLCM construction. In the left-side figure, experimental hip-knee angle phase diagram is shown. In the right-side figure, shifted hip-knee angle phase diagram and the fitting curve of $f(x_\tau)$ is shown. The form of $f(x_\tau)$ can be a polynomial, a RBF neural network or a GPR model, as introduced in subsection III.A. (b) Time histories of experimental knee angle and mapped knee angle using different candidates for subject 8 at WS3 (4.5km/h). The black solid line is the experimental data. The red, green, blue solid line is the motion-lagged GPR model, RBF network, 2-order polynomial. The red, green, blue dashed line is the corresponding candidate without motion lag.

Fig.3(b) shows the time histories of mapped knee angles with or without motion lag. One can find that the motion-lagged models all achieve good fitness for the experimental data. On the contrary, corresponding models without motion lag barely fit the experimental data. This feature can be explained by referring to the phase diagram in Fig.3(a). Before shifting the hip motion, each hip angle maps to two different knee angles, so knee angle cannot be determined only by hip angle. After shifting the hip motion with motion lag, each hip angle can map to two similar knee angles, so the mapping from hip angle to knee angle can be realized with a small

error. Therefore, motion lag is necessary for our coordination mapping. So far, the effectiveness of MLCM has been verified.

B. Comparisons With the SOTA

In this subsection, the prediction accuracy and prediction time will be evaluated for three candidates to determine the MLCM form. In addition, the MLCM will also be compared with the mapping used in [17] (as state of the art). All the calculations are completed on the computer with a CPU of Intel(R) Core(TM) i7-7700 CPU @ 3.60GHz.

The MLCM will be applied to predict knee motion at any walking speed in the real-time prosthesis controller. We hence perform leave-one-out-cross-validation (LOOCV)[14] to present our results. For the data at five walking speeds of each subject, one of the walking speeds is taken as the test set, and the other four walking speeds are used as training sets. Thus, four groups of mapping parameters can be obtained from training sets and then be averaged to act as the mapping parameters of the test set. In this way, the prediction accuracy for every walking speed of ten subjects is obtained by calculating the RMSEs between the mapped and experimental data. The average prediction RMSEs and prediction time for each walking speed are plotted in Fig.4.

Fig.4(a) shows that the MLCM shows higher accuracy (smaller RMSE) than SOTA, and the accuracy is almost the same between the GPR and polynomial candidates. The prediction accuracy slightly increases with the polynomial order, except for WS1. In terms of prediction time (Fig.4(b)), the GPR candidate costs the most, which is not conducive to the online deployment of the algorithm. Because the polynomial candidate is more straightforward and faster than other candidates, and the prediction accuracy is not sensitive to the polynomial order, we choose the polynomial of order four as the final MLCM form.

C. Relationship Between Motion Lag and MARP

For two sinusoidal signals at the same frequency with a certain phase difference, e.g.,$y = \sin(\omega t)$ and $y = \sin(\omega t + \varphi)$, the conversion between the phase difference φ in the frequency domain and the time lag τ in the time domain can be represented as $\tau = \varphi/\omega$ or

$$\tau = \varphi T/(2\pi), \tag{9}$$

where $T = 2\pi/\omega$ is the period of the sinusoidal signal. This equation inspires us to inspect the intrinsic relationship between the identified hip-knee motion lag τ and the widely used MARP.

Table S.I in Supplementary lists all the hip-knee MARPs and motion lags of all subjects at different walking speeds. By referring to Eq. (9), Fig.5 takes the independent and responding variables as MARP · T (T is the period time) and the motion lag τ, respectively. One can find that these points show obvious linear correlations, except for the data point of Subject 7 at Speed 1. This data will be discarded in subsequent analysis. The explanation for this outlier will be discussed in

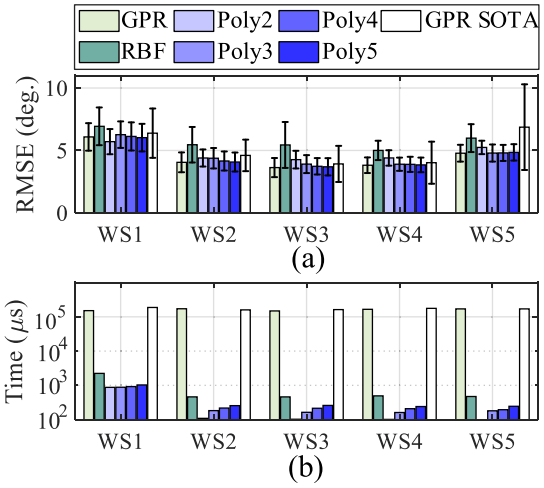

Fig. 4. (a) The RMSEs for each walking speed using different mappings, where the error bar represents the standard deviation between subjects. (b) Prediction time for each walking speed using different mappings. Polyn represents an n-order polynomial. GPR SOTA represents the model used in [17], where hip angle and angular velocity are used as inputs.

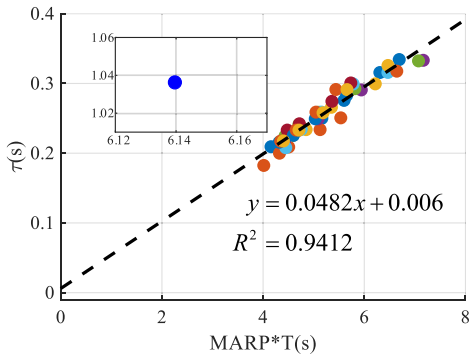

Fig. 5. Linear relationship between hip-knee phase difference and motion lag.

Section V. Using the LSM to fit these data points yields the following linear expression.

$$\begin{aligned} \tau &= 0.0482\text{MARP} \cdot \text{T} + 0.006, \\ R^2 &= 0.9412. \end{aligned} \tag{10}$$

It is not difficult to find that the curve fitting result, shown as the black dashed line in Fig.5, indicates a satisfying linear relationship between the motion lag and the hip-knee MARP. However, it is worth noting that in the sinusoidal signal, the slope of the curve should be $1/2\pi \approx 0.16$, which is distinct from our result of 0.0482. This difference remains to be studied in our follow-up research work.

This linear relationship fills the knowledge gap between the research of lower-limb coordination and the establishment of coordination mapping. It tells us the motion lag parameter introduced in the mapping is meaningful in lower-limb coordination. Instead of traversing from 0 to T to find the optimal motion lag (the method used in subsection III.A), we can obtain the motion lag by calculating the MARP and the period time. In this way, the MLCM will be practicable for the real-time control of the prosthesis.

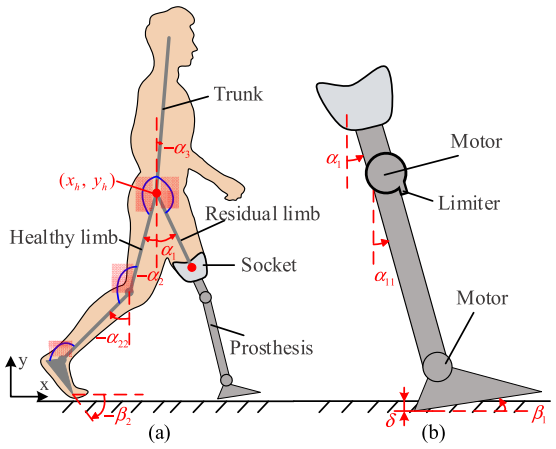

Fig. 6. Prosthesis-healthy limb heterogenous coupled model. (a) Prosthesis-healthy limb coupled system. (b) Model of the prosthesis.

IV. Application to Prosthesis Control: A Simulation Example

The MLCM established in Section IV can be used for the trajectory planning of the knee prosthesis. This section gives a control strategy for applying the mapping to generate the reference knee trajectory in real-time. To verify the effectiveness of our control strategy, we apply it to the prosthesis-healthy limb heterogenous coupled model established in our previous research [28]. The results show the potential of this control strategy in the motion of the knee prosthesis under different walking speeds.

A. Dynamic Model

As shown in Fig.6, the transfemoral amputee wearing a prosthesis is a multi-link system composed of eight segments. This system can be divided into two parts, i.e., the prosthesis and the human body. The prosthetic subsystem consists of the prosthetic thigh, the prosthetic shank, and the prosthetic foot. The human body subsystem includes the trunk, the healthy thigh, the healthy shank, the healthy foot, and the residual thigh. The prosthetic thigh and residual thigh are rigidly connected through the socket. Each foot is supposed to be triangular. The knee prosthesis and ankle prosthesis are all driven by motors. The ground reaction force governs the heel and toe of each foot. Based on the Lagrange equation of the second kind, the dynamic model of prosthesis-healthy limb coupled system can be derived as

$$\mathbf{M}(\mathbf{q})\ddot{\mathbf{q}} + \mathbf{C}(\mathbf{q},\dot{\mathbf{q}})\dot{\mathbf{q}} + \mathbf{N}(\mathbf{q}) = \mathbf{F}_e(\mathbf{q},\dot{\mathbf{q}}) + \mathbf{F}_q(\mathbf{q},\dot{\mathbf{q}}), \quad (11)$$

where $\mathbf{q} = (x, y, \alpha_1, \alpha_2, \alpha_3, \alpha_{11}, \alpha_{22}, \beta_1, \beta_2)^T$, x and y are the horizontal and vertical displacement of the hip joint, α_1 and α_{11} are the angles of the prosthesis thigh and shank relative to the vertical direction, α_2 and α_{22} are the angles of the healthy thigh and shank relative to the vertical direction, α_3 are the trunk angle relative to the vertical direction, β_1 and β_2 are the angles of prosthesis foot and healthy foot relative to the horizontal direction. All the above angles are in the counterclockwise direction. $\mathbf{M}(\mathbf{q})$ is the mass matrix, $\mathbf{C}(\mathbf{q},\dot{\mathbf{q}})$ is the Coriolis force or centrifugal force term, $\mathbf{N}(\mathbf{q})$ is the gravity term, $\mathbf{F}_e(\mathbf{q},\dot{\mathbf{q}})$ is the generalized force term generated by the foot-ground interaction force and the unilateral constraint force of the knee joint, $\mathbf{F}_q(\mathbf{q},\dot{\mathbf{q}})$ is the generalized force term caused by the healthy limb and residual limb joints, knee and ankle prosthesis motors. The form of $\mathbf{F}_e(\mathbf{q},\dot{\mathbf{q}})$ can be referred to [28]. The forms of $\mathbf{M}(\mathbf{q})$, $\mathbf{C}(\mathbf{q},\dot{\mathbf{q}})$, $\mathbf{N}(\mathbf{q})$, and $\mathbf{F}_q(\mathbf{q},\dot{\mathbf{q}})$ are given in Supplementary.

The knee motor and ankle motor are generated by PD control. The form of τ_{knee} andτ_{ankle} will be given in subsection IV.C when it comes to the control architecture of the prosthesis. After the above derivation, we have obtained the prosthesis-healthy limb heterogenous coupled dynamic model.

B. Real-Time Estimation of Motion Lag

Based on the hip-knee MLCM, we can generate the predicted knee trajectory of the prosthesis just from the hip trajectory of the healthy limb and then apply this trajectory to the position control of the knee prosthesis. In this way, only one hip motion sensor will be mounted on the residual limb for prosthesis control.

Notice that the motion lag τ in the MLCM should be estimated in real-time. According to Eq. (10), MARP and T must be obtained to calculate the motion lag in real-time. According to Eqs. (3)-(6), the calculation of MARP uses the motion data of the hip and knee, which requires the placement of sensors on the thigh and shank of the healthy limb. In addition, the calculation of MARP involves the Hilbert transform, which requires at least one cycle of gait data in advance. To avoid placing extra sensors on the healthy limb and reduce the calculation complexity of MARP, we need to establish the relationship between easily obtained real-time gait parameters and MARP. Observing Fig.1a, we consider a linear correlation between MARP and walking speed, denoted as v.

$$\text{MARP} = a_1 v + a_2, \quad (12)$$

where a_1 and a_2 are coefficients. Substituting Eq. (12) into Eq. (10) yields

$$\begin{aligned}\tau &= 0.0482a_1 \cdot v\text{T} + 0.0482a_2 \cdot \text{T} + 0.006 \\ &= A_1 \cdot v\text{T} + A_2 \cdot \text{T} + A_3, \end{aligned} \quad (13)$$

where v is the walking speed (m/s), and T is the time period (s). Using the LSM and the data of 10 subjects at five walking speeds (the data of Subject 7 at Speed 1 is discarded) for identification, we can obtain

$$A_1 = -0.0094, A_2 = 0.2547, A_3 = -0.0020.$$

It is found that the RMSE of the identified motion lag and the actual motion lag is 0.0124s, which is acceptable compared to the average motion lag (0.2570s, relative error percentage 4.82%).

So far, the motion lag will be estimated by Eq. (13) if we can obtain the walking speed and period time in real-time. The research shows that period time can be obtained according to the time interval between two heel strike moments, which are easily detected by the pressure sensor on the sole of the foot [29]. Meanwhile, A model-based method to estimate walking speed with only a shank-embedded IMU is proposed

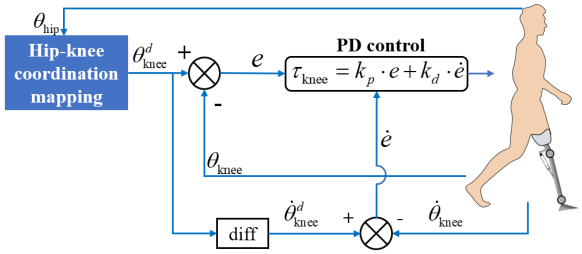

Fig. 7. Control flow chart.

TABLE IV
RMSEs Between Prosthesis Trajectory and Experimental Trajectory for Each Walking Speed

	WS1	WS2	WS3	WS4	WS5
RMSE(°)	7.84 ±1.62	7.37 ±2.22	8.26 ±2.81	8.62 ±2.62	9.61 ±1.56

in [30]. Thus, the walking speed and period time estimation can be realized by installing a pressure sensor on the sole of the prosthesis foot and an IMU on the shank of the prosthesis. Further, the motion lag can be estimated in real-time.

C. Control Architecture Based on MLCM

The control strategy flow chart is shown in Fig.7. First, the IMU sensor attached to the thigh records the hip motion signal. Then, the motion lag is calculated in real-time by Eq. (13), and the reference trajectory of the knee prosthesis θ^d_{knee} is generated by using the hip-knee MLCM. The real trajectory and angular velocity of the knee joint are measured for the feedback term of control. At last, a PD control strategy is applied to generate the knee torque, which is expressed as

$$\tau_{\text{knee}} = K_{p,\text{knee}} \cdot \left(\theta^d_{\text{knee}} - \theta_{\text{knee}}\right) + K_{d,\text{knee}} \cdot \left(\dot{\theta}^d_{\text{knee}} - \dot{\theta}_{\text{knee}}\right), \tag{14}$$

where $\tilde{\theta}_{\text{knee}}$ and $\dot{\tilde{\theta}}_{\text{knee}}$ are the reference angle and angular velocity of knee prosthesis, θ_{knee} and $\dot{\theta}_{\text{knee}}$ are the angle and angular velocity of the knee prosthesis in the simulation. $K_{p,\text{knee}}$ and $K_{d,\text{knee}}$ are set as 1275 and 60.

The ankle torque is also generated by the PD control strategy.

$$\tau_{\text{ankle}} = K_{p,\text{ankle}} \left(\tilde{\theta}^d_{\text{ankle}} - \theta_{\text{ankle}}\right) + K_{d,\text{ankle}} \left(\dot{\tilde{\theta}}^d_{\text{ankle}} - \dot{\theta}_{\text{ankle}}\right), \tag{15}$$

where $\tilde{\theta}_{\text{ankle}}$ and $\dot{\tilde{\theta}}_{\text{ankle}}$ are the reference angle and angular velocity of ankle prosthesis obtained in subsection II.A, θ_{ankle} and $\dot{\theta}_{\text{ankle}}$ are the angle and angular velocity of ankle prosthesis in the simulation, $K_{p,\text{ankle}}$ and $K_{d,\text{ankle}}$ are set as 170 and 17.

D. Control Results

Table IV shows the RMSEs between prosthetic and experimental trajectories for each walking speed. The standard deviation represents the difference across subjects. Compared with the prediction RMSE in Fig.4(a), the controlled prosthesis RMSE is more significant. This error increase is mainly caused by the contact between the prosthesis and the ground. Except for WS1, the RMSE increases with the growth of walking speed. Basically, the RMSEs maintain below 10°. The results verify the feasibility of our control strategy in simulation. Real prosthesis experiments also need to be carried out in the future.

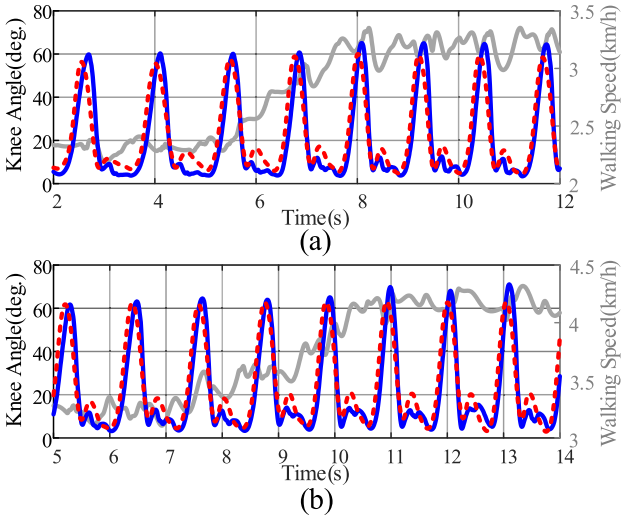

Fig. 8. The control results of knee angle (Subject 4) with changing speeds. Red dashed line for experimental knee angle, blue solid line for prosthesis knee angle obtained by PD control, gray solid line for walking speed. (a) WS1-WS2; (b) WS2-WS3. Because of the human weight and other factors, the walking speed is obtained from the speed of the heel marker during stance phase. Due to human weight and other factors, there is a certain difference between the real walking speed and the walking speed displayed by the treadmill.

Fig.8 shows the simulation results with changing speeds of Subject 4 (randomly selected). The mapping parameters take the average of five walking speeds and do not change during the simulation. Assuming that the sensor has obtained the walking speed and period time, the motion lag can be easily estimated by Eq. (13). The maximum knee angle increases significantly after speed change, which may be caused by the increase of the range of hip angle. The results show that our method is suitable for changing speed motion.

V. Discussion

A. Hip-Ankle and Knee-Ankle Coordination

In Section II, the existence of a hip-knee coordination mapping is pointed out through statistical analysis. It can be found that the performance of hip-ankle and knee-ankle coordination (MARP and DP values) is quite different among different individuals compared to that of hip-knee coordination. A reasonable explanation is that because the foot connected to the ankle joint directly contact the ground, the ankle angle is greatly affected by the foot-ground contact, making its coordination with other joints (knee-ankle and hip-ankle) relatively unstable. Thus, the coordination mappings of hip-ankle and knee-ankle are more difficult to establish than that of hip-knee. If further study wants to explore knee-ankle and hip-ankle coordination, the factor of foot-ground contact should be considered.

1) Individual Differences of MLCM: According to subsection II.D, individual differences do not easily affect the

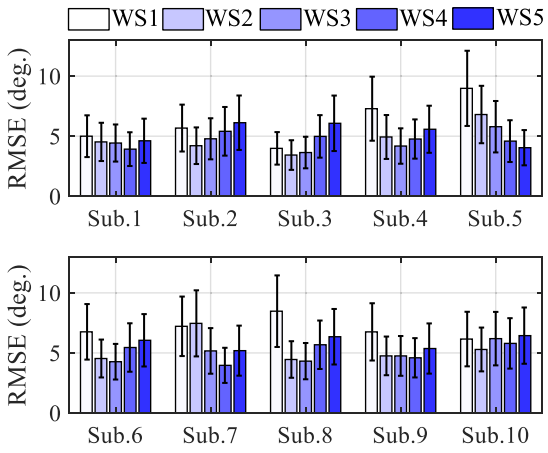

Fig. 9. The prediction RMSEs using the mapping of different subjects, where the error bar represents the standard deviation between the RMSEs obtained from the mapping of different subjects.

hip-knee coordination relationship. Thus, the hip-knee MLCM is expected to be applied to different individuals. To explore the feasibility of this idea, We apply the mapping of all other subjects to the subject's motion that need to be predicted (e.g., use the mapping of Subjects 2∼10 to predict the knee angle of Subject 1). The prediction RMSEs are shown in Fig.9. As shown in the figure, in addition to WS1 and WS5, the middle three walking speeds can achieve RMSE below 5°. This feature indicates that the mapping has a certain universality among subjects. Further research should deeply explore the relationship between the MLCM and the subject physical parameters (body segments' weight, length, etc.).

2) Relationship Between the Hip-Knee MARP and the Motion Lag: The relationship between the hip-knee MARP and the motion lag is further revealed. In sinusoidal signals, the relationship between phase difference and time lag is definite and intuitive. However, for non-harmonic signals such as hip and knee motions, the relationship between the two has never been studied. Using MARP to characterize the hip-knee phase difference and the method in subsection III.A to calculate the motion lag, we established the linear relationship between the two for the first time. Furthermore, we learned that this relationship is stable and does not change with walking speed and individual subjects. Thus, instead of qualitatively analyzing the coordination between the hip and the knee through MARP, we reveal the vital role of MARP in hip-knee coordination. Nevertheless, the deeper physical meaning of the linear relationship between the hip-knee MARP and the motion lag needs to be explored in the future.

B. An Explanation for the Excluded Data Point

In Fig.5, the data point of Subject 7 at WS1 is excluded because the motion lag is 1.0363s (see Table S.I in Supplementary material), which is distinct from other data points of the motion lag. This outlier can be explained by the relationship of reward function with motion lag shown in Fig.10. As can be seen, the reward function has two local maximal values, and these two maximal values are very close. The motion lag of Subject 7 at WS1 is obtained at the maximal value near the left end, whereas the other motion lags are picked at the maximal values near the left end. By observing the knee motion and shifted hip motion in Fig.3(a), we can find that if the motion lag is obtained at the maximal value near the left end, the hip motion translates to a state where the motion trends between the hip and the knee are basically opposite. Therefore, we can reasonably speculate that if the motion lag is obtained at the maximal value near the left end, the hip motion will translate to a state where the hip and knee motion trend is the same. This speculation can be verified in subsequent studies. For consistency of the results, when calculating the MLCM of Subject 7 at WS1, we directly take its motion lag as 0.33s.

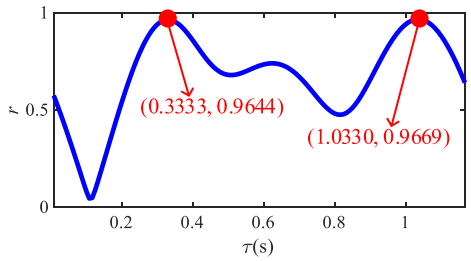

Fig. 10. Relationship of reward function r with motion lag τ for Subject 7 at WS1.

C. Limitations and Future Work

This study also has some limitations. First, gait experiments with more subjects need to be carried out. At present, the MLCM is not strictly universal among subjects (e.g., at WS1 and WS5), partly because the number of subjects for training is small. After sufficient gait experiments are conducted, the subject physical parameters (body segments' weight, length, etc.) can be considered to establish a more universal mapping. Second, this paper only studies level-ground walking. We believe that gait coordination also exists when going up/downstairs and up/down slopes. Third, gait experiments with the real prosthesis should be carried out to verify the effectiveness of our control method. The simulation in Section IV shows the potential of MLCM for the prosthesis position control with only one IMU sensor attached to the thigh. It is verified in [31] that the IMU-based hip angle estimation can typically achieve an RMSE smaller than 5°, which is acceptable for most common clinical situations according to [32]. But the actual estimation effect and control effect still need to be demonstrated through experiments.

VI. Conclusion

This study contributed to the lower-limb prosthesis control by proposing a simple and intuitive trajectory planning method, i.e., the Motion-Lagged Coordination Mapping (MLCM). The MLCM revealed a linear correlation between the MARP and the motion lag, which built a solid link from the biomechanical index to the control coefficient. Three highlighted features of the established mapping model indicate a bright prospect of employing it to control the lower-limb prosthesis. First, this model only needs hip motion sensing and

does not require integral or differential calculations. This feature saves the burden of information collection and processing. Second, the motion lag in this mapping model can be directly estimated from the period time and the walking speed. Third, the established model is suitable for different individuals and walking speeds, so far as we know. This feature implies broad adaptability to various working conditions. Therefore, it will simplify subsequent control of the lower-limb prosthesis.

REFERENCES

[1] R. Fluit, E. C. Prinsen, S. Wang, and H. van der Kooij, "A comparison of control strategies in commercial and research knee prostheses," *IEEE Trans. Biomed. Eng.*, vol. 67, no. 1, pp. 277–290, Jan. 2020.

[2] H. Zhao, J. Horn, J. Reher, V. Paredes, and A. D. Ames, "Multicontact locomotion on transfemoral prostheses via hybrid system models and optimization-based control," *IEEE Trans. Autom. Sci. Eng.*, vol. 13, no. 2, pp. 502–513, Apr. 2016.

[3] N. Aghasadeghi, H. Zhao, L. J. Hargrove, A. D. Ames, E. J. Perreault, and T. Bretl, "Learning impedance controller parameters for lower-limb prostheses," in *Proc. IEEE/RSJ Int. Conf. Intell. Robots Syst.*, Nov. 2013, pp. 4268–4274.

[4] Y. Wen, J. Si, A. Brandt, X. Gao, and H. Huang, "Online reinforcement learning control for the personalization of a robotic knee prosthesis," *IEEE Trans. Cybern.*, vol. 50, no. 11, pp. 2346–2356, Jun. 2020.

[5] Y. Wen, M. Li, J. Si, and H. Huang, "Wearer-prosthesis interaction for symmetrical gait: A study enabled by reinforcement learning prosthesis control," *IEEE Trans. Neural Syst. Rehabil. Eng.*, vol. 28, no. 4, pp. 904–913, Apr. 2020.

[6] A. L. Shorter and E. J. Rouse, "Mechanical impedance of the ankle during the terminal stance phase of walking," *IEEE Trans. Neural Syst. Rehabil. Eng.*, vol. 26, no. 1, pp. 135–143, Jan. 2018.

[7] R. Riener, L. Lunenburger, S. Jezernik, M. Anderschitz, G. Colombo, and V. Dietz, "Patient-cooperative strategies for robot-aided treadmill training: First experimental results," *IEEE Trans. Neural Syst. Rehabil. Eng.*, vol. 13, no. 3, pp. 380–394, Sep. 2005.

[8] B. Koopman, E. H. van Asseldonk, and H. van der Kooij, "Speed-dependent reference joint trajectory generation for robotic gait support," *J. Biomech.*, vol. 47, no. 6, pp. 1447–1458, 2014.

[9] J. Hong, C. Chun, S.-J. Kim, and F. C. Park, "Gaussian process trajectory learning and synthesis of individualized gait motions," *IEEE Trans. Neural Syst. Rehabil. Eng.*, vol. 27, no. 6, pp. 1236–1245, Jun. 2019.

[10] S. Y. Shin and J. Sulzer, "An online transition of speed-dependent reference joint trajectories for robotic gait training," in *Proc. IEEE 16th Int. Conf. Rehabil. Robot. (ICORR)*, Jun. 2019, pp. 983–987.

[11] C. Zou, R. Huang, H. Cheng, and J. Qiu, "Learning gait models with varying walking speeds," *IEEE Robot. Autom. Lett.*, vol. 6, no. 1, pp. 183–190, Jan. 2021.

[12] I. Mileti *et al.*, "Muscle activation patterns are more constrained and regular in treadmill than in overground human locomotion," *Frontiers Bioeng. Biotechnol.*, vol. 8, p. 1169, Oct. 2020.

[13] S. Dey, T. Yoshida, and A. F. Schilling, "Feasibility of training a random forest model with incomplete user-specific data for devising a control strategy for active biomimetic ankle," *Frontiers Bioeng. Biotechnol.*, vol. 8, pp. 1–16, Aug. 2020.

[14] V. Rai and E. Rombokas, "A framework for mode-free prosthetic control for unstructured terrains," in *Proc. IEEE 16th Int. Conf. Rehabil. Robot. (ICORR)*, Jun. 2019, pp. 796–802.

[15] H. Vallery, E. H. F. van Asseldonk, M. Buss, and H. van der Kooij, "Reference trajectory generation for rehabilitation robots: Complementary limb motion estimation," *IEEE Trans. Neural Syst. Rehabil. Eng.*, vol. 17, no. 1, pp. 23–30, Feb. 2009.

[16] H. Vallery, R. Burgkart, C. Hartmann, J. Mitternacht, R. Riener, and M. Buss, "Complementary limb motion estimation for the control of active knee prostheses," *Biomed. Tech.*, vol. 56, no. 1, pp. 45–51, 2011.

[17] M. Eslamy, F. Oswald, and A. F. Schilling, "Estimation of knee angles based on thigh motion: A functional approach and implications for high-level controlling of active prosthetic knees," *IEEE Control Syst. Mag.*, vol. 40, no. 3, pp. 49–61, Jun. 2020.

[18] D. Quintero, D. J. Villarreal, R. D. Gregg, D. J. Lambert, and S. Kapp, "Continuous-phase control of a powered knee–ankle prosthesis: Amputee experiments across speeds and inclines," *IEEE Trans. Robot.*, vol. 34, no. 3, pp. 686–701, Jun. 2018.

[19] P. Meyns, P. Van de Walle, K. Desloovere, S. Janssens, S. Van Sever, and A. Hallemans, "Age-related differences in interlimb coordination during typical gait: An observational study," *Gait Posture*, vol. 81, pp. 109–115, Sep. 2020.

[20] A. H. Dewolf, R. M. Mesquita, and P. A. Willems, "Intra-limb and muscular coordination during walking on slopes," *Eur. J. Appl. Physiol.*, vol. 120, no. 8, pp. 1841–1854, Aug. 2020.

[21] Z. Xu *et al.*, "Lower limb inter-joint coordination of unilateral transfemoral amputees: Implications for adaptation control," *Appl. Sci.*, vol. 10, no. 12, p. 4072, 2020.

[22] A. Ranavolo *et al.*, "Lower-limb joint coordination pattern in obese subjects," *BioMed Res. Int.*, vol. 2013, Dec. 2013, Art. no. 142323.

[23] P. C. Raffalt, J. A. Kent, S. R. Wurdeman, and N. Stergiou, "To walk or to run–A question of movement attractor stability," *J. Exp. Biol.*, vol. 223, no. 13, 2020, Art. no. jeb224113.

[24] M. P. Kadaba, H. K. Ramakrishnan, and M. E. Wootten, "Measurement of lower extremity kinematics during level walking," *J. Orthopaedic Res.*, vol. 8, no. 3, pp. 383–392, 1990.

[25] Y. Wang, K. Zhang, J. Zeng, and S. Yan, "Coordination of lower limbs in patients with knee osteoarthritis during walking," *Gait Posture*, vol. 83, pp. 160–166, Jan. 2021.

[26] H. Yu, T. Xie, S. Paszczynski, and B. M. Wilamowski, "Advantages of radial basis function networks for dynamic system design," *IEEE Trans. Ind. Electron.*, vol. 58, no. 12, pp. 5438–5450, Dec. 2011.

[27] Z. Liu, J. Xu, and H. Fang, "Extracting inherent model structures and identifying parameters of time-varying systems using local linear neuro-fuzzy networks," *IEEE Trans. Fuzzy Syst.*, vol. 30, no. 1, pp. 233–247, Jan. 2022.

[28] Y. Lv *et al.*, "A heterogeneous model for gait analysis of the lower-limb and the prosthesis coupled system," in *Proc. ASME Int. Design Eng. Tech. Conf. Comput. Inf. Eng. Conf.*, 2020, pp. 1–8.

[29] N. Thatte, T. Shah, and H. Geyer, "Robust and adaptive lower limb prosthesis stance control via extended Kalman filter-based gait phase estimation," *IEEE Robot. Autom. Lett.*, vol. 4, no. 4, pp. 3129–3136, Oct. 2019.

[30] B. Dauriac, X. Bonnet, H. Pillet, and F. Lavaste, "Estimation of the walking speed of individuals with transfemoral amputation from a single prosthetic shank-mounted IMU," *Proc. Inst. Mech. Eng., H, J. Eng. Med.*, vol. 233, no. 9, pp. 931–937, Sep. 2019.

[31] M. Al-Amri, K. Nicholas, K. Button, V. Sparkes, L. Sheeran, and J. L. Davies, "Inertial measurement units for clinical movement analysis: Reliability and concurrent validity," *Sensors*, vol. 18, no. 3, p. 719, 2018.

[32] J. L. McGinley, R. Baker, R. Wolfe, and M. E. Morris, "The reliability of three-dimensional kinematic gait measurements: A systematic review," *Gait Posture*, vol. 29, no. 3, pp. 360–369, Apr. 2009.